Journal of Nuclear Materials 379 (2008) 118–123

Contents lists available at ScienceDirect

Journal of Nuclear Materials

journal homepage: www.elsevier.com/locate/jnucmat

Long-term corrosion behaviour of low-carbon steel in anoxic environment: Characterisation of archaeological artefacts

M. Saheb [a,b,*], D. Neff [a], Ph. Dillmann [a,c], H. Matthiesen [d], E. Foy [a]

[a] Laboratoire Pierre Süe, UMR 9956 CEA/CNRS, bât. 637 CEA Saclay, 91191 Gif-sur-Yvette, France
[b] ANDRA, 1, rue Jean Monnet, 92298 Chatenay Malabry cedex, France
[c] Institut de recherche sur les Archéomatériaux, Laboratoire Métallurgies et Cultures, UMR 5060 CNRS, France
[d] Department of Conservation, National Museum of Denmark, IC Modewegsvej, 2800 Lyngby, Denmark

A B S T R A C T

In the context of nuclear waste storage, archaeological artefacts can be used as analogues for long-term prediction of iron corrosion behaviour. As many studies are based on laboratory simulations, it is necessary to establish a link between short and long-term behaviour. In this study, corrosion product crystalline structures on archaeological artefacts buried in soils and iron coupons immersed in synthetic environments have been compared. The occurrence of carbonated iron (siderite $FeCO_3$ and iron hydroxicarbonate $Fe_2(OH)_2CO_3$) has been observed on items from both environments using Raman microspectroscopy and X-ray micro-diffraction.

1. Introduction

In the context of French nuclear waste storage, it is planned to set up a deep geological repository for the high level radioactive waste storage. This multi-barrier system could consist in vitrified waste, steel overpack, buffer clay material and surrounding rock. The function of the steel overpack is to prevent vitrified waste from contact with groundwater for a period of thousands years. The main factor that could limit its function is the corrosion due to the contact with groundwater. During the initial stage of repository, the overpack is expected to be in relatively oxidising conditions and then to change into reducing conditions due to oxygen consumption in the corrosion reaction.

Then, the question remains of the corrosion mechanism in anoxic environments. Actually, in carbonated environments, cathodic reactions that could occur are the following [1]:

$$2H^+ + 2e^- \rightarrow H_2 \quad (1)$$

$$2H_2CO_3 + 2e^- \rightarrow H_2 + 2HCO_3^- \quad (2)$$

$$2HCO_3^- + 2e^- \rightarrow H_2 + 2CO_3^{2-} \quad (3)$$

The parameters that could influence the cathodic reaction are pH and carbon dioxide partial pressure. Whatever, the considered reaction gaseous hydrogen is formed. Then, the location of the cathodic reaction in the corrosion layer can influence the structure and reactivity of this latter. As archaeological artefacts corroded in comparable conditions are ancient systems and present thick corrosion layers, they provide efficient test samples for the study of corrosion mechanisms in anoxic media.

To this purpose, the ongoing project has been developed. Archaeological sites presenting anoxic environments are selected and corrosion layers on ferrous artefacts are studied. Moreover, as archaeological artefacts present a complex corrosion structure, iron coupons have been corroded in a synthetic environment with the same characteristic as the archaeological burial site. These samples provide a thinner corrosion layer but they are formed in a controlled environment. Thus, they will be used for preliminary tests for the localisation of the cathodic reaction in the corrosion layer. Nevertheless, in order to better understand the system under interest, a first step of the work is the corrosion layer characterisation on archaeological artefacts and on iron coupons. In this context, corrosion layer behaviour will be compared on short and long-term scale.

Iron behaviour studies in anoxic environments have been carried out in laboratory environments and therefore concern short-term corrosion mechanisms. According to literature, in anoxic carbonated environments, the most frequent corrosion product is siderite $FeCO_3$ [2–4]. Moreover, some other carbonated phases such as a green rust GR(1) CO_3^{2-} with the formula $[Fe_4^{(II)}Fe_4^{(II)}(OH)_{12}][CO_3 \cdot 2H_2O]$ [5] and iron hydroxide carbonate [6] are identified. Blengino et al. [2] have found two carbonate compounds in thin corrosion layers: siderite and iron hydroxicarbonates with the general formula $Fe_x(OH)_y(CO_3)_z$ formed from the oxidation of GR(1). These corrosion products have been identified on iron sheets immersed in a carbonated solution with a pH of

* Corresponding author. Address: Laboratoire Pierre Süe, UMR 9956 CEA/CNRS, bât. 637 CEA Saclay, 91191 Gif-sur-Yvette, France. Tel.: +33 1 69 08 23 05; fax: +33 1 69 08 69 23.
E-mail address: mandana.saheb@cea.fr (M. Saheb).

0022-3115/$ - see front matter © 2008 Elsevier B.V. All rights reserved.
doi:10.1016/j.jnucmat.2008.06.019

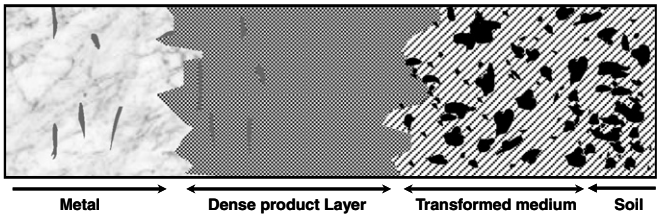

Fig. 1. Corrosion structure on iron artefacts buried in soil.

9.5 at 25, 50 and 80 °C. An iron hydroxicarbonate $Fe_2(OH)_2CO_3$ has also been identified in 1976 by Erdös and Altorfer [7] on a steel piece in an industry site. This steel piece was part of a water heater with a temperature that could increase to 180 °C. The phase has been characterised using X-ray diffraction, thermal analyses and infra-red spectroscopy. Furthermore, Savoye et al. [8] observe the occurrence of an amorphous phase $Fe(OH)_3$ containing inserted HCO_3^- and CO_3^{2-} ions that grows on thin sheets in anoxic carbonated environments at 90 °C. This phase has been characterised using Raman spectroscopy and its spectrum presents a main peak at 1070 cm^{-1}. However, the question remains on the reliable correlation between laboratory simulations and *in situ* corrosion in anoxic soils during centuries.

Few studies have been done in anoxic soils on archaeological artefacts. Previous studies show the following layer structure (Fig. 1): the metal is in contact with a thick corrosion layer (several hundreds micrometers) that contains iron corrosion products and called dense product layer (DPL) by the authors because of its higher density than the transformed medium. The transformed medium (TM) is adherent to the dense product layer and contains tracers from soil (quartz grains for example) and a high iron amount.

Analyses on archaeological artefacts have been carried out on items collected on the site of Glinet, located in Normandy (France). This site is an old industry site from the 16th century [9] and contains many small ferrous items. On the collected samples, it has been established that the dense product layer is mostly composed of siderite ($FeCO_3$) with few strips of magnetite (Fe_3O_4) and maghemite (Fe_2O_3) on the outer part [10,11]. On some samples, another iron carbonate has also been evidenced using Raman spectroscopy (occurrence of carbonate main peak at 1070 cm^{-1}).

On the one hand, studies have been carried out on iron thin corrosion layers formed during laboratory experiments in anoxic environments and on the other hand, archaeological artefacts have been studied. No link has been yet established between short-term and long-term corrosion behaviour in anoxic soils. Thus, in this study, as coupons have been corroded in synthetic environments reproducing the media at the burial site, a comparison of the corrosion layer structure of coupons and archaeological artefacts has been realised.

2. Methodology

2.1. Corpus

2.1.1. Iron coupons

Coupons used for analyses are 8 Armco iron coupons (1 × 2 cm). Their composition is available on Table 1.

Table 1
Composition of the Armco iron coupons

Element	C	S	Mn	P	Cu	N	Sn
% wt	0.003	0.004	0.050	0.004	0.007	0.0016	0.002

Iron coupons have been cleaned using a hydrochloride solution (1 M). They were then ground with SiC paper (grad 4000) and polished under ethanol until a 3 μm diamond paste.

2.1.2. Archaeological corpus

The first site that has been studied here is the one of Nydam Mose located in the South of Denmark. This site is an old sacrificial lake in which war booty was deposited as gifts for the God who ensured the victory during the Danish Iron Age, from 300 to 600 AD [12]. It has then become overgrown and has evolved into a bog. This site is of interest for several reasons. Firstly, it is equipped with already tested methods for monitoring the environmental conditions. At the depth of the archaeological artefacts, the soil is waterlogged and the oxygen concentration is below the detection limit, indicating an anoxic environment. Soil composition has been studied and Table 2 sums up the results on pH, carbon dioxide partial pressure, redox potential and water composition (averaging on 20–100 samples) [13]. Moreover, a large number of ferrous items are available, both archaeological artefacts and modern analogues that have been monitored since 1999 [14]. pH, carbon dioxide, oxygen and redox potential are measured directly in the waterlogged soil at the depth of the archaeological artefacts, whereas the other species are measured in water samples from dipwells. Structure and composition of corrosion layers on ten samples (four parts of swords and six parts of lances) excavated in 1994 and 1995 have been characterised.

In addition to that, items coming from the archaeological site of Saint-Louis (16th) have been studied. This site located in Alsace (France) is a well where several minor tools have been excavated at different depths in 2004 and 2005. The conservation state of the minor tools is variable and probably depends from the depth. It has not been possible to carry out *in situ* measurements on this site. Table 3 presents the archaeological items from the two sites that have been studied in the present work.

Table 2
Soils measurements in Nydam Mose: average on 20–100 samples

pH	[6–6.5]
Carbon dioxide partial pressure	0.3–0.5 atm
Dissolved oxygen	<0.1 mg/L
Redox potential	[−220 mV; −170 mV]
[Fe]	12 mg/L
$[SO_4^{2-}]$	21 mg/L
$[NO_3^-]$	7.8 mg/L
$[NH_4^+]$	12 mg/L
$[PO_4^{2-}]$	6 mg/L
$[Cl^-]$	37 mg/L
Alkalinity	4.6 meq/L (280 mg/L as HCO_3^-)
$[Ca^{2+}]$	160 mg/L
$[Na^+]$	24 mg/L
$[Mg^{2+}]$	7 mg/L
$[K^+]$	<2 mg/L

Table 3
Archaeological corpus

Nydam Mose (2nd–5th c., Denmark)		Saint-Louis (16th c., France)	
Name	Object	Name	Object
NM 678 (1991)	Lance	StL2004_10 (2004)	Minor tool
NM 691 (1991)	Lance	StL2004_16 (2004)	Minor tool
NM 3866 (1994)	Lance	StL2004_17 (2004)	Minor tool
NM 2931 (1994)	Lance		
NM 3958 (1994)	Lance		
NM 6356 (1995)	Sword		
NM 6531 (1995)	Sword		
NM 7105 (1995)	Sword		
NM 7627 (1995)	Sword		

As far as possible, archaeological items have been preserved from corrosion in dry air after excavation. Then, they were mounted in epoxy resin, cut, ground with SiC paper (grad 80–4000) and polished under ethanol until a 3 μm diamond paste.

2.1.3. Synthetic anoxic environment

A synthetic anoxic and carbonated environment based on Nydam Mose *in situ* measurements (see Table 2) has been created in an autoclave. An aqueous electrolyte with a composition similar to groundwater has been synthesised using various salts (Table 3) and a 0.5 atmosphere carbon dioxide partial pressure was imposed at room temperature (22 °C). Iron coupons were immerged for three months in this environment.

In this media electrochemical impedance spectroscopy measurements were carried out using a Gamry Potentiostat G750. Electrodes were low-carbon steel cylinder samples and measurements were done during three months twice a week. The applied potential varied from ±10 mV around the corrosion potential with a frequency from 0.001 Hz to 20 kHz.

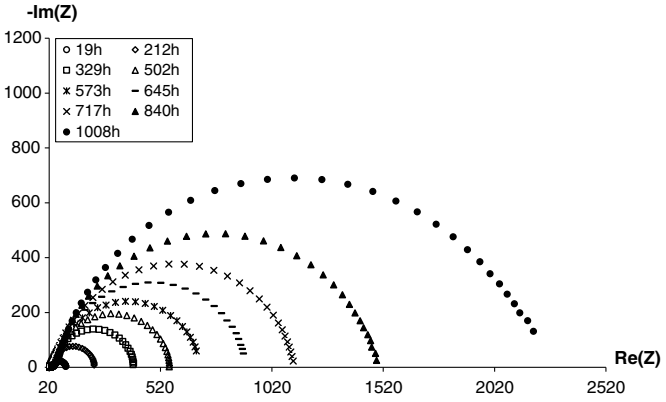

Fig. 2. Nyquist diagram on iron coupons in synthetic medium.

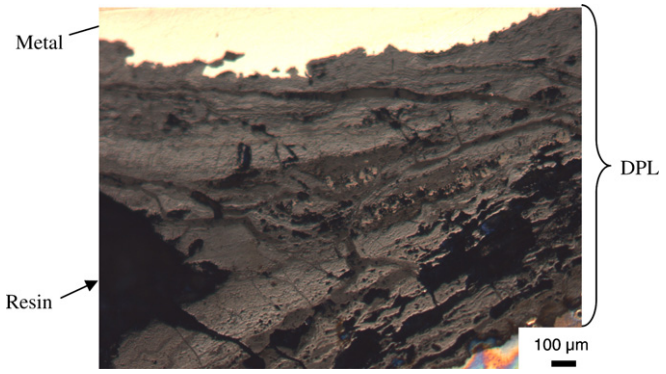

Fig. 3. Microphotograph of a transverse section on a Nydam Mose sample.

2.1.4. Corrosion layer characterisation

Microprobe techniques were used to determine the morphology, elementary composition and structure of the corrosion system. Energy dispersive spectroscopy (EDS) coupled to scanning electron microscopy (SEM) was used for observation and elementary composition analyses. Raman micro-spectroscopy and X-ray micro-diffraction (μXRD) were carried out on the samples to determine the corrosion products crystalline nature.

EDS coupled to SEM analyses were carried out using a Stereoscan 120 microscope from Cambridge Instruments (accelerating voltage: 15 kV).

Micro Raman analyses were realised with two Jobin Yvon-Horiba spectrometers (Labram Infinity and HR) delivering a 532 and a 514 nm monochromatic beam respectively. Spot size was 3 μm. The laser was filtered down to 80 μW under the 100 magnification objective since iron corrosion products are very sensitive to laser heating and can transform [3]. The spectral resolution was 2 cm^{-1}. The phases were identified by comparison with powder standards and data given by literature [3,15].

X-ray micro-diffraction analyses were performed using a photon microprobe built on a rotating anode X-ray generator. The beam delivered by a molybdenum anode (K_α: 17.45 keV) was first monochromatised by a torroïdal multilayer mirror and then focused on a surface of 20 × 20 μm^2 through a borosilicate monocapillary. μXRD patterns were collected in transmission mode downstream the thin film sample (100 μm) by a 2D image plate detector. Classical $I = f(2\theta)$ powder μXRD patterns were obtained after circular integration of the diffracted image using the FIT2D program [16].

Classical XRD analyses were performed on an X-ray diffractometer using a HT generator (PW 3040) and a cobalt X-ray source (PW 3376/00 Co LFE). Analyses were carried out in $\theta/2\theta$ mode.

3. Results and discussion

3.1. Iron coupons corrosion layers

Corrosion layer growth on iron coupons in synthetic anoxic environment has been followed using electrochemical impedance spectroscopy measurements as shown on the Nyquist diagram on Fig. 2.

The polarisation resistance increased with immersion time which revealed a corrosion film growth. After three months, a 4 μm thick corrosion layer was obtained. Its structure has been analysed using XRD and Raman micro-spectroscopy.

The XRD highlights the fact that the corrosion layer was composed of siderite. Moreover, peaks from another corrosion product

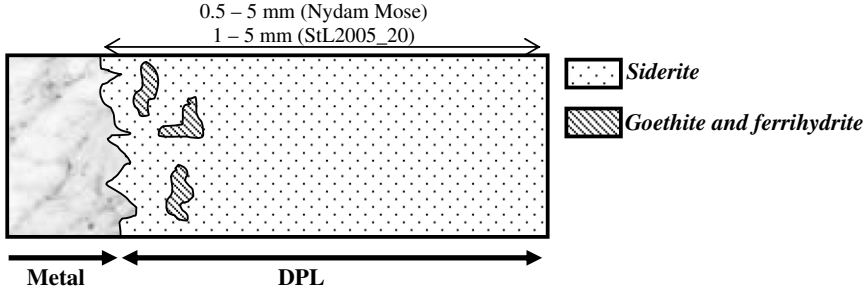

Fig. 4. Corrosion diagram on Nydam Mose samples and StL2004_17.

were also evidenced. The reference pattern with the better agreement to the collected XRD diagram corresponded to the iron hydroxicarbonate $Fe_2(OH)_2CO_3$. (JCPDF number: 33-0650) [7]. These analyses have been completed using Raman micro-spectroscopy on transverse sections (see Fig. 6). The inner part of the corrosion layer was mainly composed of siderite $FeCO_3$ (main Raman peak at 1084 cm^{-1}) while the outer part is an iron carbonate that could be the hydroxicarbonate $Fe_2(OH)_2CO_3$ (main Raman carbonate peak at 1071 cm^{-1}). These results were in good agreement with XRD analyses.

3.2. Archaeological artefacts corrosion layer

Archaeological artefacts were buried in complex anoxic systems in which environmental parameters present variations. Consequently, different corrosion layouts were observed on the items. Results have been classified into three types.

3.3. First corrosion layer type: siderite matrix, goethite and ferrihydrite

The items providing from Nydam Mose site were cleaned before storage; consequently, no transformed medium (TM) was left on them. On the ten samples, the same corrosion products morphology was observed and identified.

DPL thickness was between 0.5 and 5 mm and the layer was constituted of a dark matrix with lighter zones (around 10 μm wide). Moreover, cracks parallel and perpendicular to the metal/corrosion products interface have been observed through the entire thickness. Fig. 3 represents a microphotograph of the corrosion system developed on a sword coming from Nydam Mose site.

Calcium, phosphorus and sulphur have been identified in the DPL as soil tracer elements (<4 wt%). The structural analyses revealed a main phase constituted of siderite and corresponding to the dark phase on microphotograph. Moreover, lighter zones corresponding to goethite (α-FeOOH) or ferrihydrite [3] were locally present in the DPL. Concerning these both oxi-hydroxides, a doubt about their formation during the burial period can be entertained. They could have precipitated from a phase transformation or from a corrosion restart after excavation.

On the minor tool from Saint-Louis StL2005_20, the same corrosion layout has been identified as on Nydam Mose items.

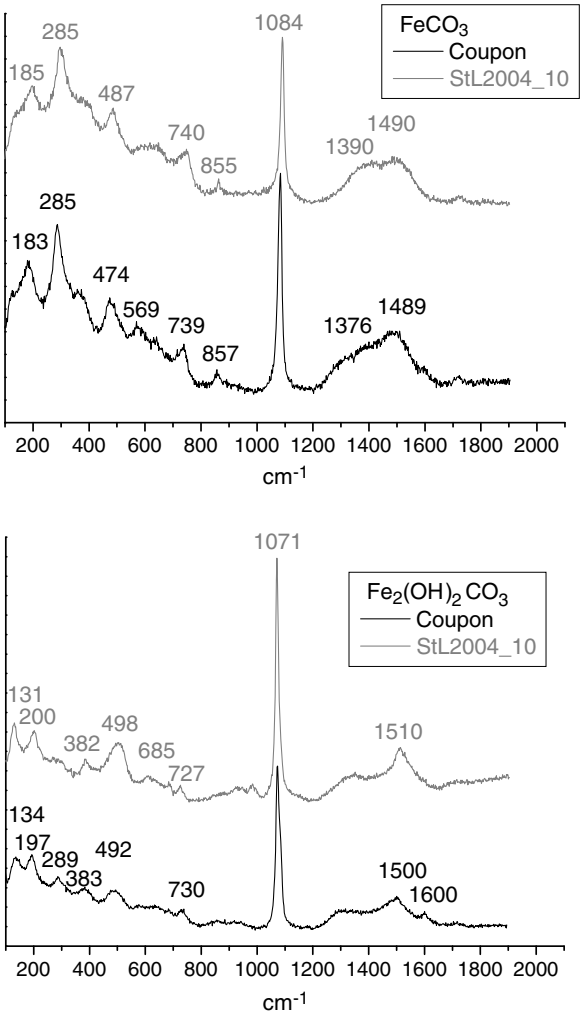

Fig. 6. Raman spectra on iron coupons and StL2004_10, $\lambda = 514$ nm.

Two zones were present: an internal zone, heterogeneous and between 1 and 3 mm thick. This zone was composed of a mixture of

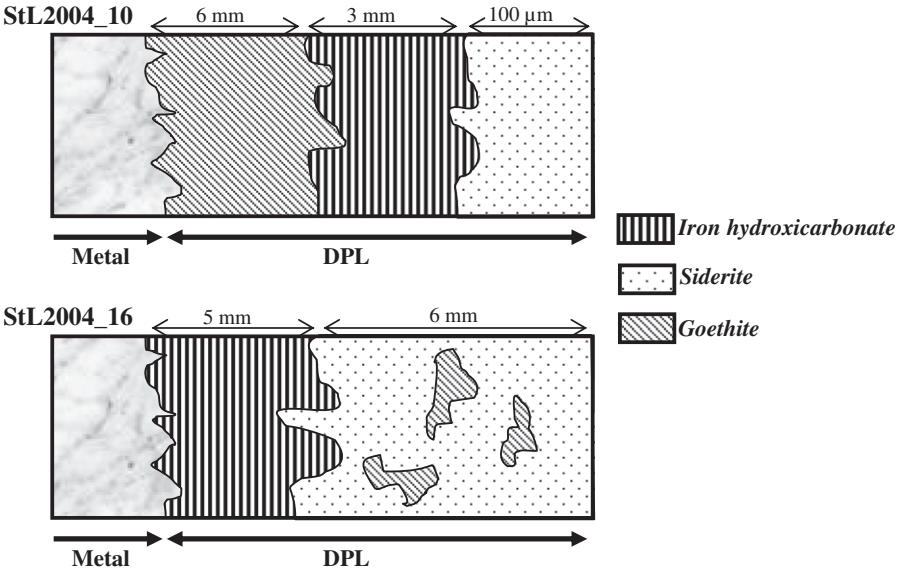

Fig. 5. Corrosion diagram on StL2004_10 and StL2004_16.

siderite and goethite. Surrounding it, a dark layer (0.5–2 mm) appeared homogenous and contained siderite. In this case the occurrence of a mixture of goethite and siderite on the internal part could be explained by an alternation of wet and dry periods during the burial.

Corrosion diagram of observed samples containing both siderite and goethite is presented on Fig. 4.

3.4. Second corrosion layer type: siderite, iron hydroxicarbonate and goethite

On two minor tools (StL2004_10 and StL2004_16), the co-occurrence of siderite, iron hydroxicarbonate and goethite was observed. In every DPL, an iron hydroxicarbonate $Fe_2(OH)_2CO_3$ was located on the internal part, whereas siderite $FeCO_3$ was on the external part as it is presented on Fig. 5. The inner layer was a mixture of goethite (identified using μXRD) and ferrihydrite (identified using μRaman).

In the case of StL2004_10, goethite was directly in contact with the metal contrary to the StL2004_16, where this phase was present in localised zones inside the siderite zone. The occurrence of this corrosion product on StL2004_10 identified in the case of aerated environments could be explained by corrosion phenomena that could have occurred before the tools were embedded in soil. On StL2004_16, the occurrence of goethite on the external zone of the DPL could be the result of a phase transformation after excavation or the consequence of changes in the burial environment.

3.4.1. Comparison between corrosion layer structure on iron coupons and archaeological artefacts

On iron coupons, two carbonate phases have been identified: siderite $FeCO_3$ and iron hydroxicarbonate $Fe_2(OH)_2CO_3$. Raman microspectra of these two phases are presented in Fig. 6 and compared to the one observed on StL2004_10 minor tool. For both phases, very similar Raman signals were obtained on archaeological and modern items.

Moreover, Fig. 7 presents the XRD diagram obtained on the surface of an iron coupon and the μXRD diagrams obtained on each siderite and iron hydroxicarbonate zones of the StL2004_10 minor tool. The use of two analytical set-ups could explain the different peak width. However, the peak positions were the same with both tools. Consequently, a good match between corrosion products on the archaeological artefacts and on the coupons was obtained. Corrosion products have been identified using comparison to reference patterns ($Fe_2(OH)_2CO_3$:JCPDF: 33-0650 [7] and $FeCO_3$:JCPDF: 29-0696).

From these results it is obvious that the anoxic carbonated environments were suitable for the formation of carbonated iron corrosion products, such as siderite and hydroxicarbonate. However, it has to be questioned, if the corrosion products formed on the coupons are representative of what was formed on the archaeological site. Indeed the synthetic solution aimed at reproducing Nydam Mose conditions but on the archaeological samples of this site no iron hydroxicarbonate was detected. Several reasons could generate this discrepancy. Firstly, corrosion layer identification in natural burial and in synthetic environment could be faulted due to environment changes during analyses. Actually, Nydam Mose artefacts have been excavated and then stored 10 years before analyses; it is then possible to imagine phase transformation happening inside the DPL. To prevent these transformations, samples have to be freshly excavated and placed in an inert environment protected from air. Another reason could be the synthesis of the immersion solution. Indeed iron have been dissolved in water from iron chloride $FeCl_3$. Consequently, Fe(III) was introduced in the medium, which can increase the corrosion rate by being an oxidising agent, where the reduction of Fe(III) to Fe(II) can act as an extra cathodic reaction. It can be questioned if the oxidation degree of iron could have induced the formation of different corrosion products as the one observed on archaeological items. In the future the solution will be synthesised utilising a Fe(II) compound (Mohr salt $(NH_4)_2Fe(SO_4)_2 \cdot 6H_2O$) in order to determine the influence of this parameter during the immersion of the coupons in solution.

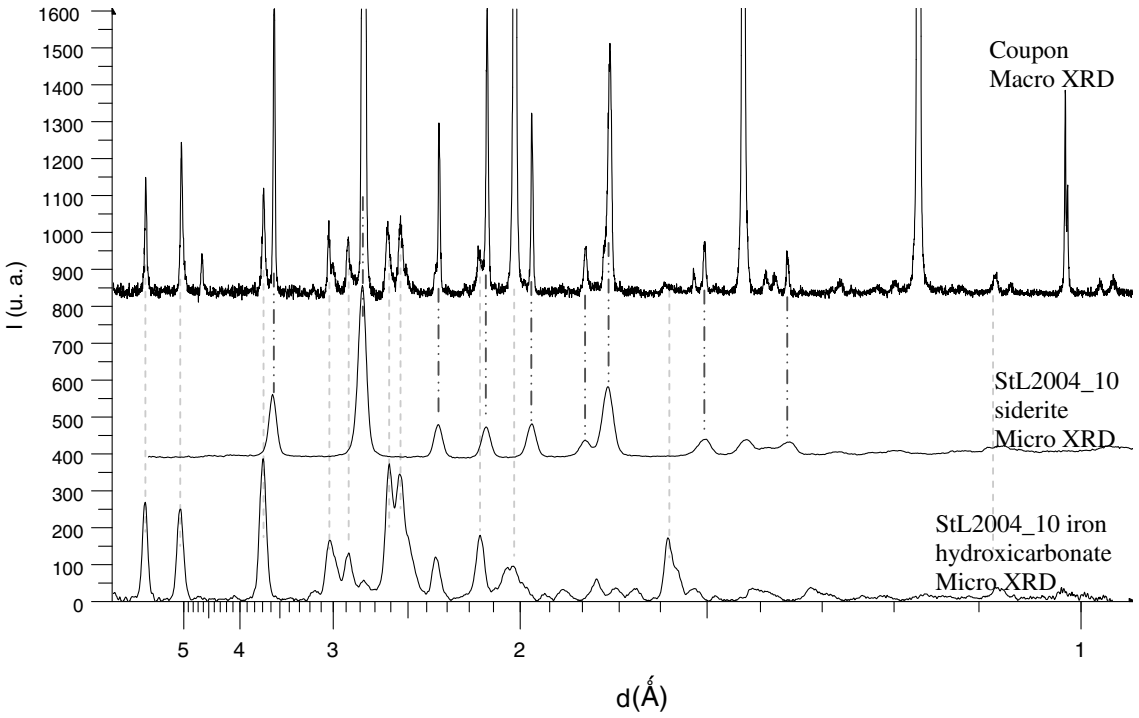

Fig. 7. X-ray diagrams collected on iron coupon and on StL2004_10 minor tool.

Table 4
Composition of the synthetic water

pH	6.3
Carbon dioxide partial pressure	0.5 atm
[Fe]	20 mg/L
$[SO_4^{2-}]$	23 mg/L
$[NO_3^-]$	15 mg/L
$[Ca^{2+}]$	10 mg/L
$[K^+]$	8 mg/L
$[Cl^-]$	42 mg/L

4. Conclusion and prospects

In the presented work, a comparison between the corrosion layer crystalline structure formed on the one hand on ferrous archaeological artefacts collected in anoxic soils and on the other hand iron coupons corroded in laboratory has been established.

On archaeological artefacts, an iron carbonate has been identified; siderite $FeCO_3$ which is representative of iron corrosion in anoxic carbonated media. Moreover, on some samples, an iron hydroxicarbonate $Fe_2(OH)_2CO_3$ has been identified on the internal part of the corrosion layer. On iron coupon, both phases, siderite on the external part and iron hydroxicarbonate on the internal part have been identified.

The aim of the laboratory simulations was to reproduce the burial environment of the Nydam Mose archaeological site. However, on Nydam Mose samples, no iron hydroxicarbonate has been identified in the corrosion products. Then, the study highlights the difficulty to simulate an anoxic burial environment in laboratory. Indeed, in the presented study, iron under Fe(III) form was used for the synthesis of the electrolyte. In the future experiments, the electrolyte will be synthesised using iron Fe(II). This will allow for a better simulating the burial medium.

Moreover, to avoid phase transformation during analyses, samples will undergo a special preparation. Concerning archaeological artefacts, freshly excavated items will be analysed. They will be excavated with part of the burial environment present and stored in absolute ethanol. Then the artefacts will be mounted into resin under vacuum. Archaeological items and coupons will be cut and polished in a glove box under nitrogen flux. With all these cautions, the oxygen influence will be minimised. Corrosion products characterisation will be compared to the one observed on the items sampled in contact with air (see Table 4).

The presented paper is part of an ongoing project concerning iron corrosion mechanism in anoxic environments. Archaeological artefacts and iron coupons will be used as test samples for identifying reaction localisation in corrosion layers. To this purpose, anoxic deuterated burial environment will be synthesised. Formed deuterated phases will be then localised inside the corrosion layer with Raman micro-spectroscopy and nuclear microprobe.

Acknowledgements

This work is financially supported by the ANDRA and the French Agence Nationale de la Recherche ANR program ARCOR. Moreover, we thank Alex Chenière for his help during the XRD analyses, Ludovic-Bellot-Gurlet for the μRaman analyses and Clarisse Mariet and Francine Carrot for the HPLC measurements. Electrochemical measurements have been realised with precious help of Christian Bataillon, Pierre Vigier and Stéphane Perrin. Moreover, we thank the archaeologists who supplied the samples, Danielle Arribet-Deroin and Patrick Clerk.

References

[1] J.K. Heuer, J.F. Stubbins, Corros. Sci. 41 (1999) 1231.
[2] J.M. Blengino et al., Corros. Sci. 37 (1995) 621.
[3] D. Neff et al., J Raman Spectrosc 37 (2006) 1228.
[4] M. Reffass et al., Corros. Sci. 48 (2006) 709.
[5] P. Refait, J.M. Génin, Corros. Sci. 34 (1993) 797.
[6] M.C. Bernard et al., Prog. Org. Coat. 45 (2002) 399.
[7] E. Erdös, H. Altorfer, Werkst. Korros. 27 (1976) 302.
[8] S. Savoye et al., Corros. Sci. 43 (2001) 2049.
[9] D. Arribet-Deroin, in: Archéologie, Paris I Sorbonne, Paris, 2001, p. 799.
[10] D. Neff et al., Corros. Sci. 47 (2005) 515.
[11] E. Vega, Altération des objets ferreux archéologiques sur le site de Glinet (Seine-maritime, France, XVIe siècle). Caractérisation des produits de corrosion et étude des mécanismes., Université de Technologie de Belfort Montbéliard, Belfort, 2004. 127.
[12] E. Jorgensen, P. Vang Petersen, in: L. Jorgensen, B. Storgaard, L.G. Thomsen (Eds.), The Spoils of Victory – The North in the Shadow of the Roman Empire, National Museum of Denmark, 2003, p. 258.
[13] H. Matthiesen et al., J Wetland Archaeol 4 (2004) 55.
[14] H. Matthiesen et al., in: Prediction of Long Term Corrosion Behaviour in Nuclear Waste Systems, Nice, 2004, p. 114.
[15] D.L.A. de Faria, S.V. Silva, M.T.D. Oliveira, J Raman Spectrosc 28 (1997) 873.
[16] A.P. Hammersley, FIT2D Reference Manual, ESRF International Report No. EXP/AH/93-02, 1993.